The Astrophysical Journal, 592:580–589, 2003 July 20

PROPERTIES OF FAST SUBMILLIMETER TIME STRUCTURES DURING A LARGE SOLAR FLARE

Jean-Pierre Raulin, Pierre Kaufmann,[1] Carlos G. Giménez de Castro, and Alessandra A. Pacini
CRAAM, Universidade Presbiteriana Mackenzie, São Paulo, Brazil; raulin@craam.mackenzie.br

Vladimir S. Makhmutov
Lebedev Physical Institute, Leninskij Prospect, 53, Moscow GSP-1, Russia

Hugo Levato
Complejo Astronomico El Leoncito, Casillo de Correo 467, San Juan 5400, Argentina

and

Marta Rovira
Instituto de Astronomia y Física del Espacio, Casilla de Correo 67, Sucursal 28, Buenos Aires 1428, Argentina
Received 2002 October 15; accepted 2003 April 6

ABSTRACT

We report properties of fast varying submillimeter emission during one of the strongest solar radio flares of solar cycle 23. Emission was obtained by the Solar Submillimeter-Wave Telescope at 212 and 405 GHz and compared with hard X-ray and γ-ray counts up to few tens of MeV photon energy ranges. We employ different methods to detect and characterize flux density variations and find that during the impulsive phase of the event, the closer in time to the peak flare, the higher the occurrence of the fastest and brightest time structures. The good comparison with hard X-ray and γ-ray count rates indicates that fast submillimeter pulses are the signatures of primary energetic injections. The characteristics of the fast spikes at 212 and 405 GHz, such as their flux density and localization, compared to those of the underlying slower impulsive component, also suggest that their nature is different.

Subject headings: gamma rays: bursts — Sun: flares — Sun: radio radiation

1. INTRODUCTION

Particle acceleration is an important problem of solar flare physics (see, e.g., Benz 1987; Vilmer 1987; Melrose 1994; Vlahos 1995). Processes involved can be better constrained by studying the most direct diagnostics of the energetic particles that are produced during solar events: hard X-ray/γ-ray and high-frequency radio emissions. The former is expected when high-energy electrons interact with the dense material of the low solar atmosphere producing nonthermal bremsstrahlung photons. On the other hand, high-frequency radio emission results from the synchrotron emission from the same electrons as they travel through high magnetic field regions (Ramaty 1969; Dulk & Marsh 1982; Dulk 1985; Ramaty et al. 1994). Both diagnostics are complementary, and, in principle, by comparing them one should better understand the mechanism of energization of the emitting particles, as well as the processes that govern their transport through the solar corona (Ramaty et al. 1994).

It has long been recognized that microwave solar bursts are composed of variations of different timescales ranging from subseconds up to a few tens of minutes (for reviews see Kundu 1965; Krüger 1979; Kundu & Vlahos 1982; Kaufmann 1996). At higher frequencies (millimeter-wave range) selected events studied with high time resolution and high sensitivity have shown fast time structures of the order of 30 ms (Kaufmann et al. 1985; Zodi Vaz et al. 1987) and strengthened the need for even higher frequency solar observations (Kaufmann et al. 1986). Similar results were obtained using the wavelet decomposition method at microwaves (Kurths & Schwarz 1994) and at millimeter waves (Giménez de Castro et al. 2001). More recently a Solar Submillimeter-Wave Telescope (SST) was installed in the Argentinean Andes to detect the emission from the most energetic electrons produced during solar flares (Kaufmann et al. 2001b). During two X-class flares, rapid (few hundred millisecond) time variations were detected showing an increasing flux density spectrum in the submillimeter-wave (at 212 and 405 GHz) range (Kaufmann et al. 2001a, 2002), along with a main (slower) flare component due to the synchrotron emission of $\geq$10 MeV electrons (Trottet et al. 2002).

The 2001 August 25 flare occurred at location S17 E34 in NOAA Active Region 9591, at $\sim$16:30 UT, and was classified as optical class 3B, *GOES* (1–8 Å) class X5.3, with intense Hα emission detected between 16:24 and 19:17 UT (NOAA Space Environment Center and Solar-Geophysical Data bulletins). Magnetic configuration of the active region was classified as $\beta\gamma\delta$, and it was composed of two large sunspots whose umbrae were located within the same penumbra. In terms of radio emission this flare is probably one of the strongest of the present solar cycle, since it produced at the peak time $\geq 10^4$ SFU at 405 GHz and $\geq 10^5$ SFU at 89.4 GHz (J.-P. Raulin et al. 2003, in preparation), which is comparable to the large X-class events of 1991 June (Ramaty et al. 1994). We present observational characteristics of high time resolution submillimeter-wave data for the above-mentioned flare and compare them to hard X-ray (HXR) and γ-ray emissions simultaneously obtained up to the 10–100 MeV photon energy range (§ 3). In § 4 we discuss the results obtained, and we conclude in § 5.

[1] Also part-time at CSS, Universidade Estadual de Campinas, Campinas, SP, Brazil.

2. INSTRUMENTATION

2.1. *Submillimeter Instrumentation*

The SST observes the Sun at 212 and 405 GHz with six independent total power receivers (channels 1–4 at 212 GHz, and channels 5 and 6 at 405 GHz), with a time resolution of 1 ms providing a sensitivity (rms noise system temperature) of ~3 K. The multiple-receiver focal array produces a cluster of four beams (2–5) overlapping at approximately half-power beamwidth (HPBW ~ 4′ and 2′ at 212 and 405 GHz, respectively) projected on the solar disk, while the other two beams (1 and 6) are projected at a remote (~6′) site (see, e.g., Fig. 1 in Kaufmann et al. 2002). This beam disposition allows us to estimate, at each time, the location of the centroid of emission for a small (compared to HPBW) emitting source, which is used subsequently to compute the source flux density. Antenna tracking measure is monitored and is smoother than 0.″36. On 2001 August 25, SST beams 2–5 were tracking NOAA AR 9591 where the flare occurred. The atmospheric zenith opacity was estimated to be ~0.58 and ~2.6 nepers at 212 and 405 GHz, respectively, and was used to correct the raw records. Data are calibrated several times a day using known load ambient (300 K) and hot (430 K) temperatures. Linearity of the square law detectors is determined using a precision step attenuator inserted in the main IF amplifier.

The sensitivity of the 212 and 405 GHz observed signals, or minimum detectable antenna temperature at these frequencies, is governed by the system noise temperature $T_{\rm sys}$, the bandwidth of the receivers ($\Delta f = 1$ GHz), and the time constant t. The level of rms noise fluctuations is expressed by the well-known equation

$$\Delta T = \frac{T_{\rm sys}}{\sqrt{t\Delta f}} \ . \tag{1}$$

The system noise temperature $T_{\rm sys}$ accounts for the temperature of the receivers $T_{\rm rec}$, as well as for all temperatures of sources located along the line of sight: the sky, the quiet Sun, and eventually a localized burst, such that

$$T_{\rm sys} = T_{\rm rec} + T_{\rm sky}\left(1 - e^{-\tau/\sin{\rm El}}\right) + \eta T_{\rm QS} e^{-\tau/\sin{\rm El}} + T_{\rm burst} e^{-\tau/\sin{\rm El}} \ , \tag{2}$$

where τ is the zenith opacity in nepers, El is the elevation angle of the Sun, and η is a coupling coefficient between the actual solar disk brightness temperature and the observed temperature (approximately equal to the beam efficiency when the antenna is observing a source of size larger than a few HPBWs). To evaluate the relative importances of the noise temperature terms in equation (2) and their influence on the final rms noise fluctuations in equation (1), we know that $T_{\rm rec} \sim 3000$ K and take a "mean" sky temperature $T_{\rm sky} \approx 280$ K. The quantities $\eta T_{\rm QS}$ have been tabulated for the SST (Melo et al. 2002) and are in the range 1700–2400 K at 212 GHz, depending on the beam used, and 2400 K at 405 GHz. For the day of the present observation we have $\tau \sim 0.58$ and 2.6 nepers at 212 and 405 GHz, respectively. At the time of the flare the Sun elevation was El = 48°. This means that the quiet-Sun contribution term to the system noise temperature, equation (2), was in the range 780–1100 K (212 GHz for different channels 2, 3, and 4) and 72 K (405 GHz for channel 5). The excess temperature noise due to the burst $T_{\rm burst} e^{-\tau/\sin{\rm El}}$ has been estimated in the increasing part of the event at 16:31:10 UT (in the range 800–1900 K for different channels at 212 GHz and 15 K at 405 GHz for channel 5), at peak maximum at 16:31:35 UT (70 K at 405 GHz), and during the decreasing part of the event at 16:32:10 UT (in the range 1600–3900 K at different 212 GHz channels and 10 K at 405 GHz). Noise rms fluctuations due to the different contributions to the system noise temperature, i.e., receiver (R), sky (S), quiet Sun (QS), and solar burst (B), have been estimated with $t = 5$ ms and are reported in Table 1 at 212 (channels 2, 3, and 4) and 405 GHz.

Examination of Table 1 shows that the 212 GHz rms noise fluctuations for different channels, ΔT, increased by a factor ≤ 2 as a result of the flare emission, compared to the preflare value. Similarly, at 405 GHz, ΔT increased by at most 2% compared to the preflare level of ~1.5 K. The values of ΔT at 212 and 405 GHz, shown in Table 1, will be used in the next section to discuss the significance of the fast pulses observed during the main phase of the flare. However, Table 1 already informs us that the flare emission at 405 GHz did not produce any significant increase of the rms noise fluctuation level and that at 212 GHz the corresponding increase was negligible compared to the temperature fluctuations due to solar burst pulsations, as will be shown later.

2.2. *Hard X-Ray/γ-Ray Instrumentation*

HXR and γ-ray data were obtained from the Wide Band Spectrometer (WBS) on board the Japan/US/UK *Yohkoh* satellite (Yoshimori et al. 1991). HXR and γ-ray count rates were provided by the WBS/GRS-PC and WBS/GRS-PH detectors, with a time resolution in the range 0.25–4 s. These data were calibrated and analyzed using SolarSoft procedures.

TABLE 1

NOISE RMS FLUCTUATIONS (IN K) DUE TO SYSTEM NOISE TEMPERATURE CONTRIBUTIONS OF THE RECEIVERS (R), THE SKY (S), THE QUIET SUN (QS), AND THE BURST EMISSION (B)

	212 GHz			405 GHz
CONTRIBUTION	Channel 2	Channel 3	Channel 4	CHANNEL 5
R	...	1.34	...	1.34
R + S	...	1.41	...	1.46
R + S + QS	1.90	1.74	1.76	1.5
R + S + QS + B (16:31:10 UT)	2.26	2.59	2.14	1.5
R + S + QS + B (16:31:35 UT)	...	...	...	1.53
R + S + QS + B (16:32:10 UT)	2.60	3.48	2.52	1.5

3. THE PRESENCE OF SUBMILLIMETER FAST TIME STRUCTURES

In Figure 1 we show the overall flux density time profile of the event at 212 and 405 GHz, using a time constant of $t = 20$ ms, derived from antenna aperture efficiencies measured for the period of observations using planets of about 0.2 at 212 GHz and 0.13 at 405 GHz. At the top, we excluded from the 212 GHz temporal curve the time interval during which at least one of the three (2, 3, or 4) SST beams saturated. Below, we show a scalogram that illustrates the decomposition of the 212 GHz flux density curve using the wavelet transform method (Mallat 1989; Bendjoya, Petit, & Spahn 1993). The next two frames show the same as the previous two panels but at 405 GHz. For the submillimeter time profiles we also show a thick vertical bar indicating the

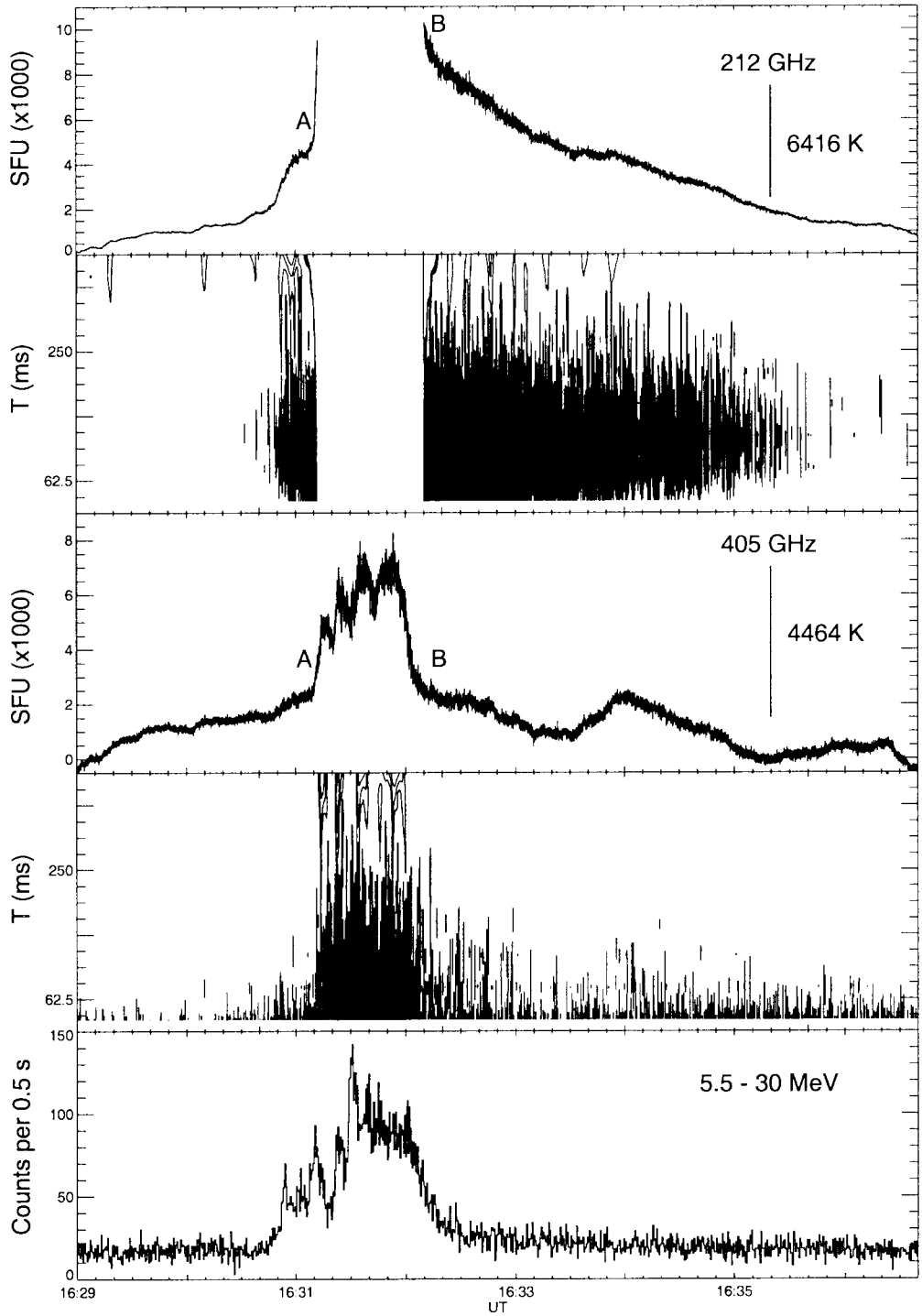

FIG. 1.—Flux density time profiles at 212 (*top*) and 405 GHz (*third panel from top*) compared with scalograms obtained at the same frequencies (*second and fourth panels from top*). We show at 212 and 405 GHz a vertical scale indicating the level of observed antenna temperatures corrected for atmospheric opacity and for burst position. Time resolution shown is 20 ms. The bottom panel shows γ-ray counts in the range 5.5–30 MeV from the *Yohkoh*/GRS spectrometers and using 0.5 s time resolution.

scale of the observed antenna temperatures obtained by channel 3 at 212 GHz and channel 5 at 405 GHz. In the bottom panel we compare with the γ-ray count rate obtained in the photon energy range of 5.5–30 MeV. The flux curves at 212 and 405 GHz show a spiky behavior starting from the fast impulsive phase of the flare until ~16:35 UT. This fast temporal behavior is significant in comparison to the rms system noise, as will be discussed with greater details in the next paragraph. The scalograms further indicate the spiky nature of the flux curves by showing the presence of rapid fluctuations from 16:30:40 UT at both 212 and 405 GHz. Their occurrence rates increase as the flare progresses.

At 405 GHz we note a good correspondence between the presence of fast varying emission and the γ-ray time profile. In particular, between 16:31:15 and 16:32:20 UT corresponding to the main emission in the γ-ray curve, we note the presence of more intense, rapid, and frequent 405 GHz time structures. At 212 GHz fast time variations are detected up to ~16:35 UT, that is, a few minutes after the peak of the event and when the greater than 5.5 MeV γ-ray time profile has vanished. Both scalograms indicate that fast pulses were detected at 212 and 405 GHz with durations as low as can be inferred by the time constant used ($2t = 40$ ms).

In Figure 2 we show examples of details of the uncorrected antenna temperature time profiles. This was done in order to illustrate submillimeter fast spikes detected at 212 (channel 3) and 405 GHz (channel 5), in the rising (label A in Fig. 1) part of the event (*third and fourth panels from top*) and during the decreasing (label B in Fig. 1) part (*bottom panels*). The same fast time structures are found for 212 GHz channels 2 and 4, with different uncorrected antenna temperatures (see Fig. 6). We also compare with the preflare emission (*top two panels*). The fifth panel from the top shows the emission observed at 405 GHz near the flare maximum, when the 212 GHz signal was saturated. Data are shown using time constants of 5 and 20 ms (overlaid using a thick line). We numbered at both frequencies some of the fast time structures during time periods A and B. On the left-hand side of each panel we show, as a thick vertical bar, the quantity $3\Delta T$, i.e., 3 times the corresponding rms system noise temperature fluctuations as calculated in the previous section and reported in Table 1. We also quote their values in kelvins, so that the observed temperature fluctuations can be directly compared with $3\Delta T$. As a result of this comparison, Figure 2 shows that during the event (time periods A and B, as well as in the peak flare time), the observed fast variations are highly significant. In particular, at 212 GHz they are of the order of 20–100 times the rms noise fluctuations. At 405 GHz observed temperature fluctuations are 2–5 times the rms noise fluctuations during A and B, and up to 10 times during the peak of the flare. We note also a good similarity between the emission at both frequencies, with an almost one-to-one correspondence between the significant fast time structures: for example, 405 GHz time structures 1, 3, 6, 7, 9, and 13 during time period A, and time structures 13, 15, 17, and 18–25 during time period B. Figure 2 exhibits an occurrence rate as high as 6–7 s^{-1}, as suggested earlier by the scalograms in Figure 1.

In conclusion, most of the submillimeter fast time structures shown in Figure 2 are significant and in general detected at both frequencies. We also note that the quantity $3\Delta T$ deduced from equation (1) and shown at the left of each panel is close to the peak-to-peak noise level visible in the observed antenna temperature time profiles, as it should roughly be.

A flux density for the above-reported fast pulses has been estimated from the excess antenna temperature signals observed with SST beams 2, 3, and 4, outside the saturation period. For each beam the excess signal was obtained by subtracting a lower envelope determined using a method based on running mean calculations (Raulin et al. 1991). We found that during the rising phase excess flux densities are $\leq$100 SFU and about 200–300 SFU at 212 and 405 GHz, respectively. In the decreasing part of the flare, 212 GHz excess flux variations are comparable to those detected at 405 GHz. The durations of the fast time variations are of the order of few tens of milliseconds and up to 200 ms for the longest ones.

We used a peakfinder-based algorithm (Raulin et al. 1998) to detect, characterize, and count all the observed fast time structures at 212 and 405 GHz, above a certain threshold defined in relation to the preflare noise level. Once a peak is detected, we can estimate its amplitude, as the difference between its peak flux and the flux at the preceding minimum, as well as its duration. As the time of each structure is known, it is easy to estimate their rate (in units of T^{-1}) of occurrence, as the number of fast structures counted within time intervals of duration T. The results are shown in Figure 3 at 212 (*top panel*) and 405 GHz (*third panel*) and compared with HXR (*second panel*) and γ-ray (*bottom panel*) time profiles. In Figure 3 we compare the flux density time profile (*thick line*) with the occurrence rate (*histogram*) of the fast structures that were detected and their amplitude variations with time (*spiky line*). As shown in Figure 2, occurrence rates reach 6–7 and 3–4 fast structures per second at 212 and 405 GHz, respectively. Faster rates might be present also at 405 GHz and could be detected if the signal was less noisy. We note that the amplitudes of the fast pulses are closely related to HXR and γ-ray count rates and match better than their occurrence rates. This is particularly evident at 212 GHz, where occurrence rates of fast pulses (independently of their amplitude) remain nearly constant at ~6 s^{-1} until 16:35 UT, while at this time HXR emission already vanished. On the other hand, the amplitudes of fast 212 GHz pulses gently decrease as does the 0.27–1 MeV time profile, which suggests a relation between the rate of the brightest fast structures detected at 212 and 405 GHz and the production of HXRs and γ-rays.

To better show the above observational properties, we used the wavelet coefficients deduced from the decomposition of the original records at 212 and 405 GHz. These coefficients, $d_{j,k}$, obtained for different timescales k and times j, represent the amplitude of the fast structures with similar timescale. Figure 4 shows how the γ-ray (above 10 MeV) profile compares with the coefficients $d_{j,k}$ obtained at 405 (*left-hand panels*) and 212 GHz (*right-hand panels*) for three particular timescales (80, 160, and 320 ms). For the analysis at 212 GHz we used the output data obtained with SST beam 1 (pointed ~6′ away from the active center), since it observed the solar burst through sidelobes, then highly attenuated, but without any saturation. Figure 4 confirms that the amplitude of fast submillimeter time structures is very well correlated with the γ-ray count rates. Between 16:32:10 and 16:32:20 UT we note a sharp decrease of the amplitude of the fast spikes, along with a similar decrease in the γ-ray signal. After that time we still see significant time structures at both frequencies, as also indicated by the

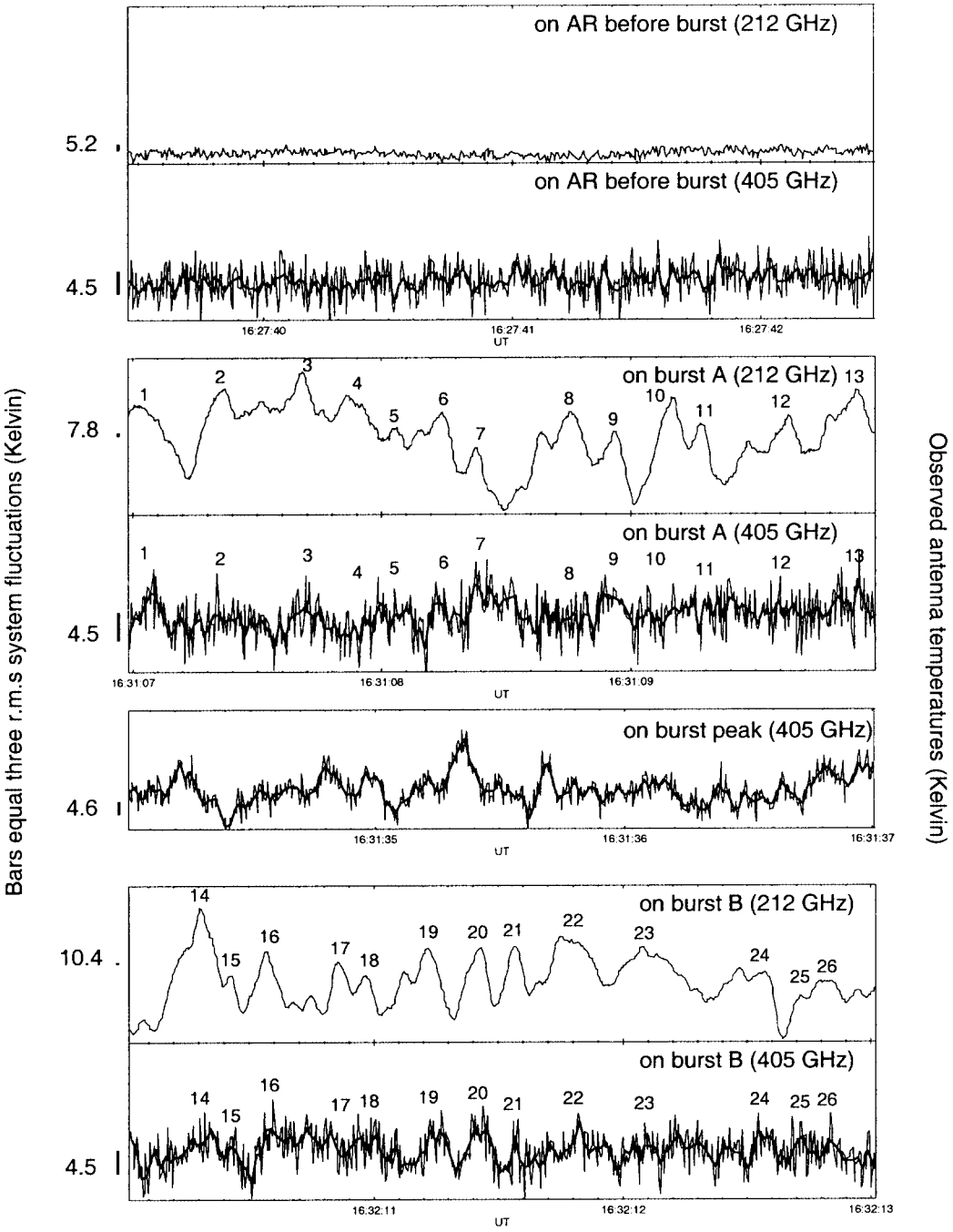

FIG. 2.—Detailed views of rapid variations in observed uncorrected antenna temperature at 212 (for channel 3; *third and sixth panels*) and 405 GHz (for channel 5; *fourth, fifth, and seventh panels*), for 3 s time intervals labeled A and B in Fig. 1 and at the peak (405 GHz), using 5 ms (20 ms: *thick line*) time resolution data. For comparison we show, in the top two panels, 212 and 405 GHz emission before the event. Vertical thick bars on the left-hand side of each panel correspond to 3 times the rms noise fluctuations ΔT, with ΔT indicated in Table 1.

occurrence rate curves shown in Figure 3, although less intense than during the main γ-ray emission.

4. DISCUSSION

In the present study we concentrated on the properties of the fast time structures that were detected during the impulsive phase of the event, as well as on their comparison with the high level of HXR and γ-ray emissions observed. A detailed multifrequency (1–405 GHz range) analysis of the main flare component, in relation to the dynamics of the active region magnetic structures, is being published elsewhere (J.-P. Raulin et al. 2003, in preparation).

Both the direct detection method and the wavelet decomposition analysis have shown that the event is composed of a hierarchy of temporal scales: few minute time variations as revealed by the main component emission at submillimeter waves between 16:30 and 16:33 UT, variations of a few seconds up to 10 s during the impulsive phase, and subsecond fast pulses (as shown in Fig. 2). These different timescales do not appear in a random way during the event, but their occurrence and duration rather seem to vary in time

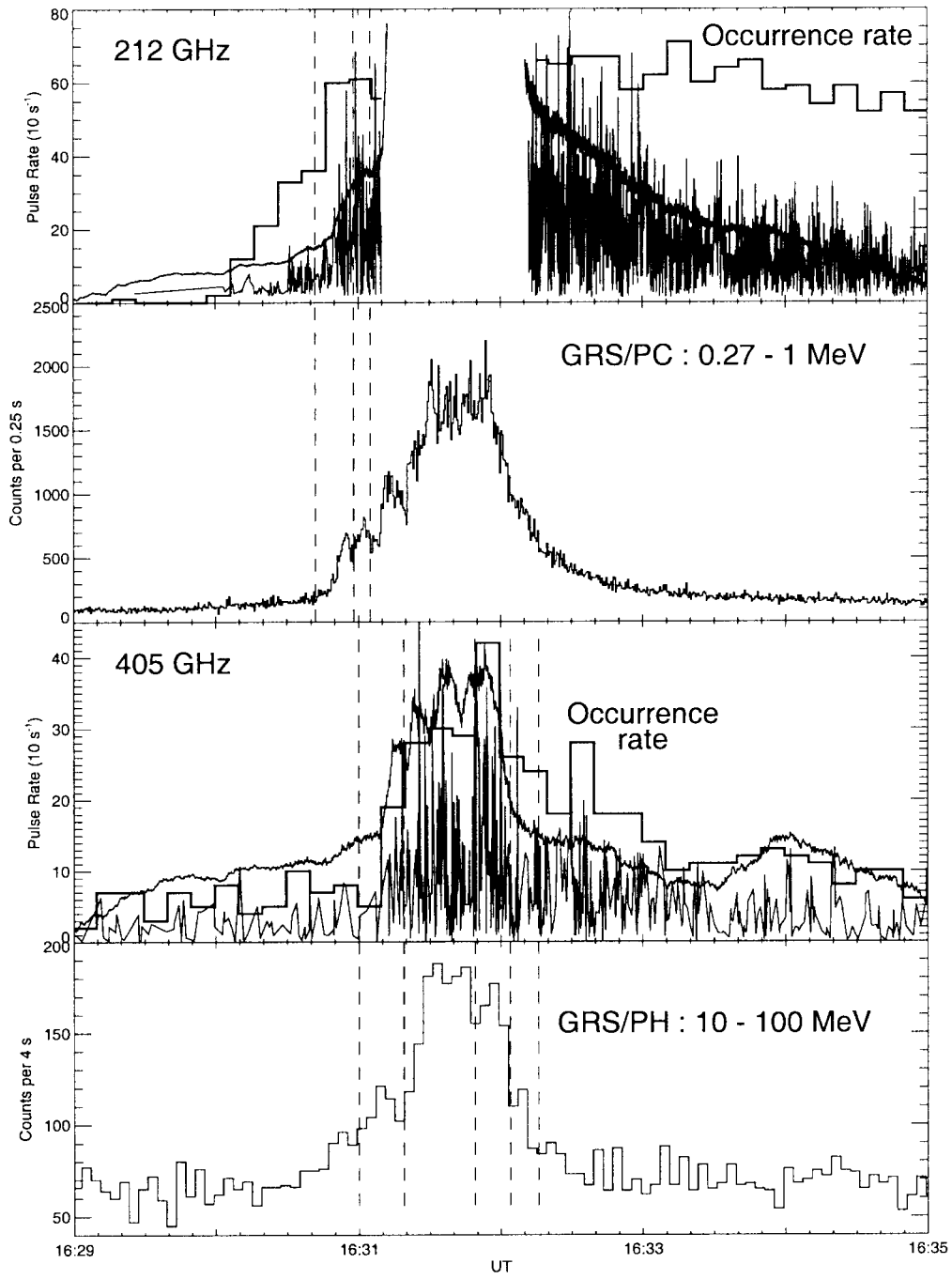

FIG. 3.—*Top two panels:* Pulse rate (*histogram*), pulse amplitude (*spiky curve*), and flux density (*thick solid curve*) at 212 GHz, compared with HXR (0.27–1 MeV) time profile. *Bottom two panels:* Same for 405 GHz and γ-ray (10–100 MeV) count rates. Vertical dashed bars show minima in the HXR and γ-ray time profiles.

within the different phases of the event. For example, scalograms at 212 and 405 GHz (Fig. 1) have shown that the fastest time structures, with duration down to $2t = 40$ ms, occur during the more energetic part of the event, in close association with HXR and γ-ray time profiles. Similarly, the time evolution of the wavelet coefficients (Fig. 4) indicates that the brightest submillimeter structures appear between 16:30:30 and 16:31:55 UT, during which time interval the flare is more intense at all wavelengths. Such behavior for fast radio pulses, although not discussed, has been reported at 90 GHz (Kaufmann et al. 1985; Correia et al. 1987), where 90 GHz fast variations appeared as trains of multiple subsecond ($\geq$0.03 s) pulses. At 48 GHz also it has been shown that the fastest and brightest time structures were detected preferentially at times of flux maxima (Giménez de Castro et al. 2001). This indicates that the characteristics of fast submillimeter variations present structural changes during the impulsive phase. Moreover, the different timescales do not seem to form a continuum (from short to long timescales, for example), but many times shorter timescales appear as disconnected from the underlying longer timescale structures. Such changes through the flare time history

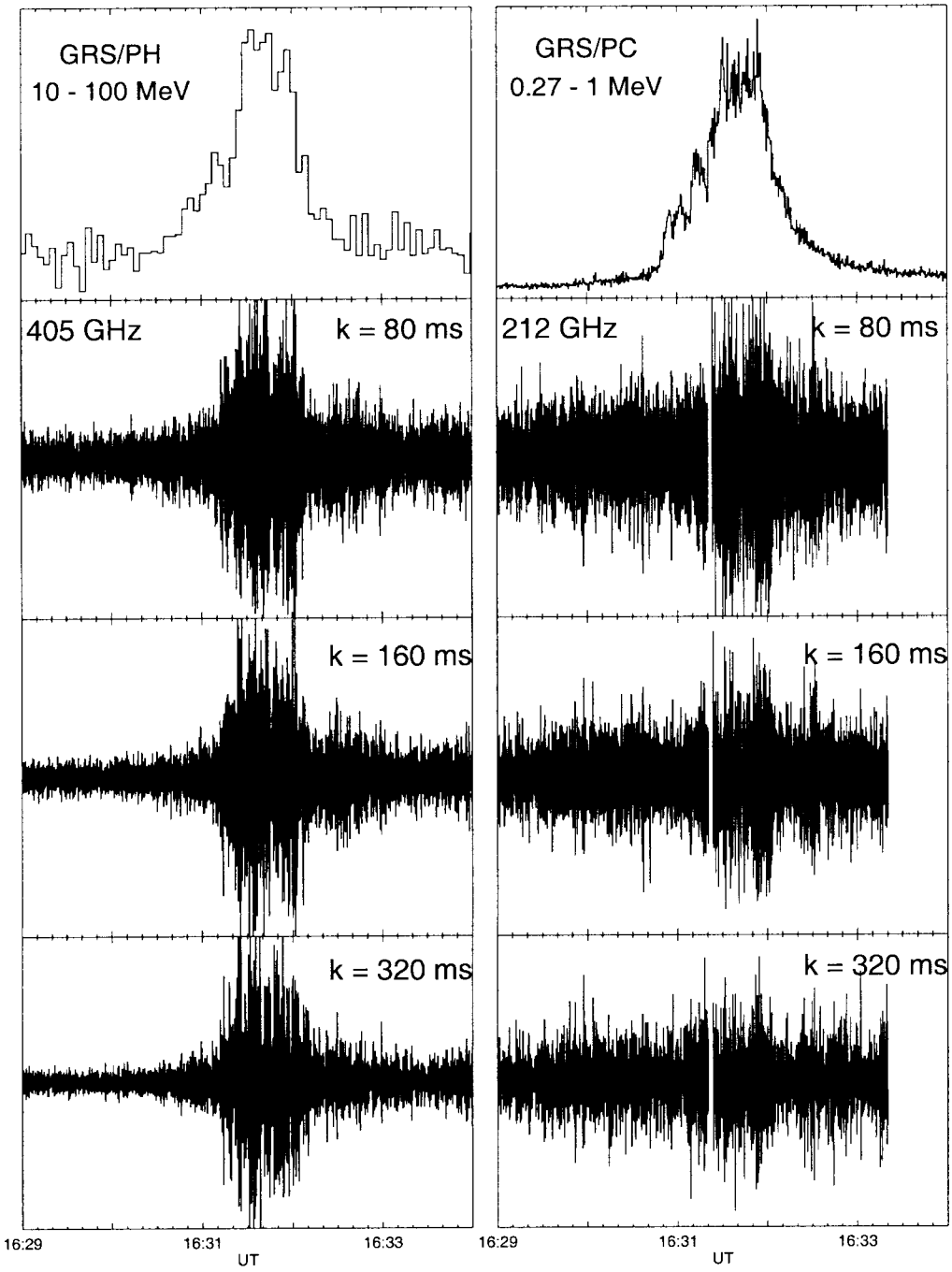

FIG. 4.—Comparison of γ-ray and HXR time profiles (*top panels*) with the time evolution of the wavelet coefficients $d_{j,k}$ for three particular timescales k: 80, 160, and 320 ms, at 212 (*right*) and 405 GHz (*left*).

are being reported and studied in more detail elsewhere for this event, as well as for other submillimeter events observed by the SST (Makhmutov et al. 2003).

A property deduced from Figures 3 and 4 is that the time profiles of the pulse amplitudes match quite well the HXR and γ-ray light curves. This means that high-energy γ-rays were produced in close connection with the fastest, more intense, and more frequent submillimeter time structures. In Figure 5 we compare the 10–100 MeV count rate with the temporal evolution of $d^2_{j,k}$ for the same three particular timescales as shown in Figure 4. At each time, $d^2_{j,k}$ represents the power found in the signal by the wavelet decomposition method in structures of timescale k. The excellent agreement shown in Figure 5 confirms that high-energy photons may have been the response to frequent and intense submillimeter pulses, which thus could reveal discrete primary energetic injections. Similar results were obtained at 212 GHz (Kaufmann et al. 2002), showing a close relation between γ-ray emission and occurrence rate of fast radio pulses. For that particular event high atmospheric attenuation prevented the detection of fast variations at 405 GHz in contrast to the event studied here. The good agreement between spike amplitudes at 405 GHz and γ-ray time profiles is also an indication that the higher the frequency of observation the closer the diagnostic to the flare primary energy releases.

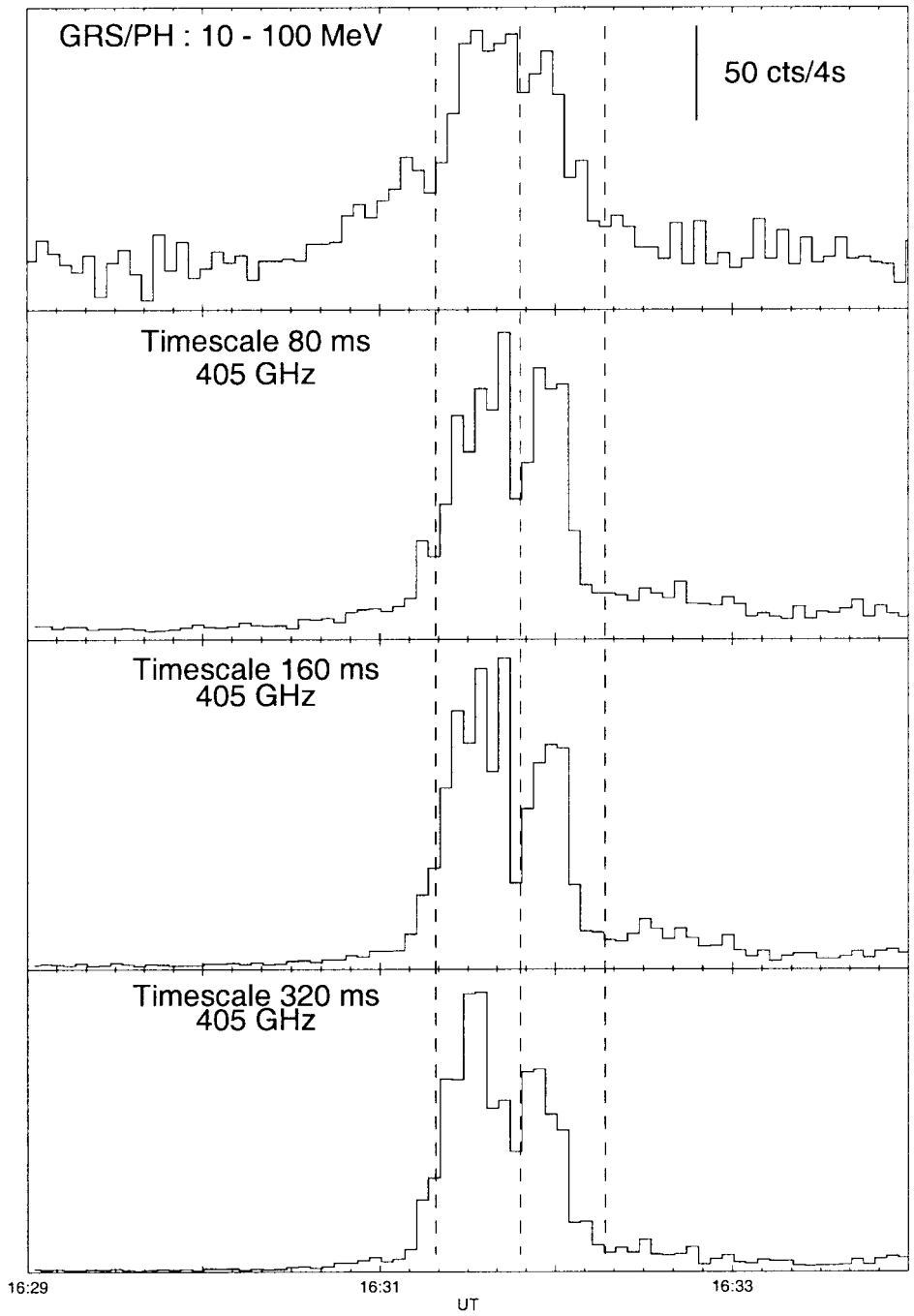

FIG. 5.—Comparison of γ-ray time profile (*top*) with that of $d^2_{j,k}$ for three particular timescales k: 80, 160, and 320 ms, at the frequency of 405 GHz

Figures 3, 4, and 5 have shown that the flare emission can be decomposed in different components, the fastest one being the rapid submillimeter spikes superimposed on top of a slower (tens of seconds) timescale emission. Often, the fastest structures appear separated from the underlying time-extended emission. This raises the question about the relation between the different timescales observed during the flare and whether they are related or originated independently from different processes. In the latter case we should then expect to detect fast time structures irrespective of the importance of the main flare component. This, in turn, might explain why, in the three X-class flares studied until now with the SST (Kaufmann et al. 2001a, 2002; Trottet et al. 2002; the present event), the fast excess flux density variations at submillimeter wave varied within a factor of 2, while the main synchrotron emission differed by a factor $\geq$500. Another solar flare under study (2001 December 13) also indicates the presence of submillimeter-wave activity in the form of fast and intense pulses without significant slower underlying emission. We also cannot exclude the possibility that part, or all, of the main component flare emission might be due to trapped particles that were injected at the time of the fast submillimeter pulses, part of them directly precipitating as indicated by the good correlation with HXR/γ-ray emissions. Then the relative importance of the different flare components could

vary depending on the local physical conditions. A similar idea has been proposed for HXR emission (Aschwanden, Schwartz, & Dennis 1998).

In the present suggested scenario the fast pulses observed at submillimeter wavelengths appear as a powerful diagnostic of the primary energy releases, associated to the production of HXRs and γ-rays in the low solar atmosphere, while the main flare emission can result from slower processes governed by the transport of energetic flare particles, like trapping. A further analysis of the main flare component focused on the transport of the fast electrons is underway.

The location of fast time structures at 212 GHz has been estimated from the original antenna temperature excess records obtained with different channels of the SST (Giménez de Castro et al. 1999), as that shown in Figure 6 (*top panel*) during time period B. The structures are similar and time coincident in 212 GHz channels 2, 3, and 4, well above the respective radiometers' noise as shown before, making the 212 GHz outputs almost noise-free signals. Therefore, the antenna temperatures for the different channels are dependent on the source position with respect to the three beam centers. Burst locations have been estimated and averaged, during 10 ms around their peak time, and compared with the position of the main underlying emission (indicated with an "M" in Fig. 6). For time period B (Fig. 6, *bottom right panel*) we also show the approximate locations of beams 2, 3, 4, and 5 (*right, left, top, and middle circles, respectively*). The effect of the rms system noise temperature fluctuations on the burst positions lies in the ranges [$-2''$; $2''$] and [$-7''$; $7''$], depending on the burst fast structure considered, and is indicated for each source by a cross around its mean position. Note that an advantage of the multiple-beam technique is that small variations in antenna pointing, resulting in three independent antenna temperature time profiles for each 212 GHz channel, will not produce apparent shifts for a single emitting source at a stable position, as described in Makhmutov et al. (1998). Figure 6 reveals that the fast pulse locations, indicators of primary energy release

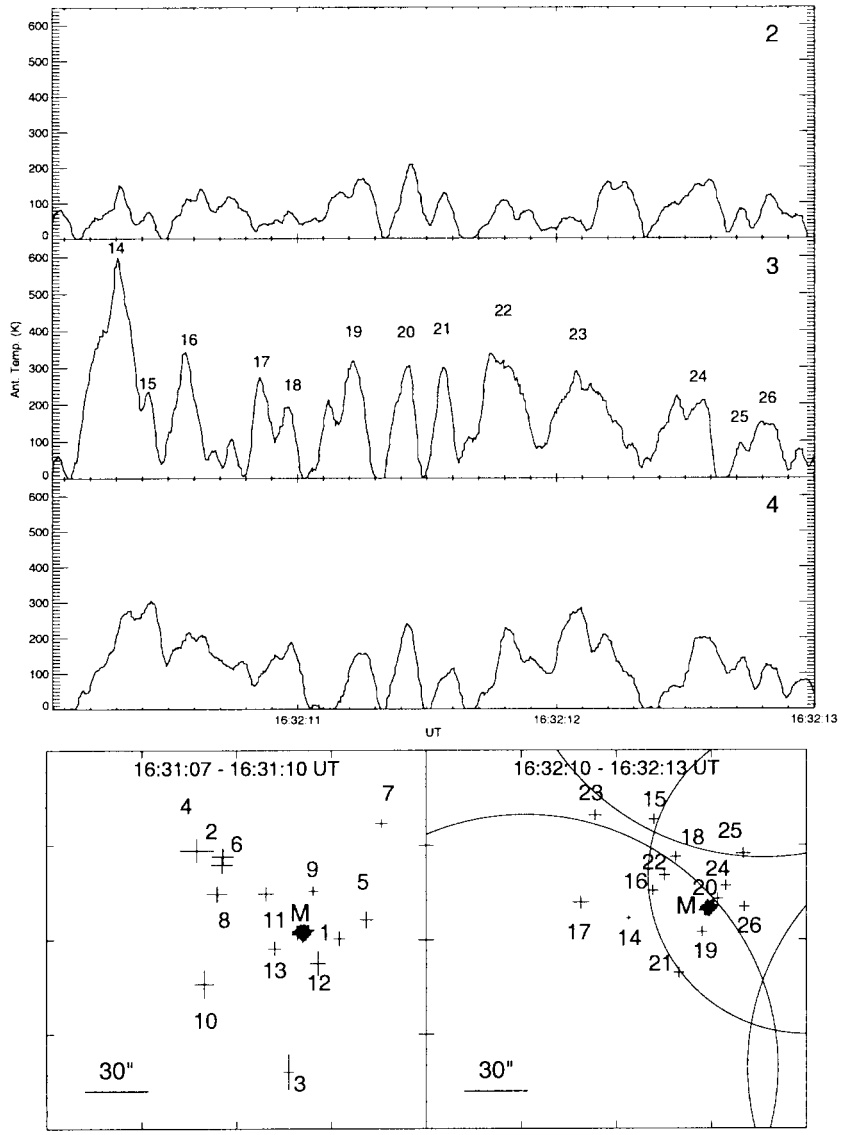

FIG. 6.—Position of the individual submillimeter-wave bursts shown in Fig. 2, averaged during 10 ms at the peak of each burst (*bottom panels*). The size of the box is $3' \times 3'$, and the absolute uncertainty on the position determination is about $30'' \times 30''$. M is the position of the underlying bulk emission component. For each fast structure the size of the cross shows the uncertainty of the position determination due to rms system noise temperature fluctuations. For the time period B burst positions are compared with the beam locations (see text). At the top we show the excess antenna temperature time profiles, obtained from channels 2, 3, and 4, and which have been used to compute the pulse positions.

sites, appear to be discrete and stationary in space (5″–15″), spread over the entire active region area. In particular, close in time (within 150 ms) fast time structures may be distant by more than 30″ [as pulses (10, 11) during time period A and pulses (1, 2) and (4, 5) during time period B, for example], as already observed at 212 GHz (Kaufmann et al. 2002) and at millimeter wavelengths (Correia et al. 1995; Raulin et al. 1998). Thus, the present findings are in favor of models that expect multiple instabilities at different locations, like multiple explosive magnetic islands (Sturrock & Uchida 1981), multiple coalescence instabilities (Tajima, Brunel, & Sakai 1982), or interaction of multiple magnetic fluxes across the active region (Tarbell & Title 1977; Sturrock et al. 1984).

We finally note that the present observations confirm that the fast time variations show higher flux densities at 405 GHz than at 212 GHz, i.e., a spectrum that increases in the submillimeter range (Kaufmann et al. 2001b, 2002). Although some attempts have been made to understand such radio spectra (Kaufmann et al. 1986; McClemments & Brown 1986), clearly more work needs to be done to understand the physical origin of the submillimeter-wave pulses. However, the properties shown in this paper and the fact that the rapid spikes are not located at the same position in space as the main component emission might be another suggestion that their nature is different from the underlying slower impulsive component.

5. CONCLUSIONS

In this paper we presented new properties of submillimeter observations obtained during one of the strongest radio events of solar cycle 23, which occurred on 2001 August 25. Numerous rapid (roughly a few tens of milliseconds to ~200 ms) pulsed (a few per second) activity has been detected at 212 and 405 GHz, whose characteristics suggest that they are closely related to the production of high-energy X-ray– and γ-ray–emitting photons. The high-frequency activity reported at 212 and 405 GHz by the SST thus appears as a diagnostic of the primary flare energy releases. The positions of the submillimeter spikes superimposed onto the main flare component are discrete and spread within the whole active region extension. This supports the idea that the primary flare energy release region is composed of multiple, discrete, and compact sites, highly variable in time (Raulin et al. 2000). Because the location of elementary radio bursts inside magnetic active centers is an important input to understand the plasma instabilities responsible for the release of energy during flares, we should expect new and relevant information by comparing spatially resolved and high-sensitivity submillimeter flare activity obtained by the SST with high energy and high spectral resolution of simultaneously obtained data and provided by the recently launched RHESSI experiment.

This research was partially supported by Brazilian agencies FAPESP (contracts 99/06126-7 and 01/00604-6) and CNPq (contracts 300782/96-9 and 304822/89-2), as well as Argentina agency CONICET. We are grateful for the support of CASLEO engineers and technicians at the observatory of El Leoncito. We also thank the *Yohkoh* team and M. Yoshimori for providing us with the WBS data. The *Yohkoh* mission of ISAS was prepared and operated by an international collaboration of Japanese, US, and UK scientists.

REFERENCES

Aschwanden, M. J., Schwartz, R. A., & Dennis, B. R. 1998, ApJ, 502, 468
Bendjoya, Ph., Petit, J.-M., & Spahn, F. 1993, Icarus, 105, 385
Benz, A. O. 1987, Sol. Phys., 111, 1
Correia, E., Costa, J. E. R., Kaufmann, P., Magun, A., & Herrmann, R. 1995, Sol. Phys., 159, 143
Correia, E., Kaufmann, P., Costa, J. E. R., Zodi Vaz, A. M., & Dennis, B. R. 1987, in SMM Topical Workshop on Rapid Fluctuations in Solar Flares, ed. B. R. Dennis, L. E. Orwig, & A. L. Kiplinger (NASA Conf. Proc. 2449; Washington, DC: NASA), 161
Dulk, G. A. 1985, ARA&A, 23, 169
Dulk, G. A., & Marsh, K. A. 1982, ApJ, 259, 350
Giménez de Castro, C. G., Raulin, J.-P., Makhmutov, V. S., Kaufmann, P., & Costa, J. E. R. 1999, A&AS, 140, 373
Giménez de Castro, C. G., Raulin, J.-P., Mandrini, C. H., Kaufmann, P., & Magun, A. 2001, A&A, 366, 317
Kaufmann, P. 1996, Sol. Phys., 169, 377
Kaufmann, P., Correia, E., Costa, J. E. R., & Zodi Vaz, A. M. 1986, A&A, 157, 11
Kaufmann, P., Correia, E., Costa, J. E. R., Zodi Vaz, A. M., & Dennis, B. R. 1985, Nature, 313, 380
Kaufmann, P., et al. 2001a, ApJ, 548, L95
———. 2001b, Telecomunicações, 4, 18
———. 2002, ApJ, 574, 1059
Krüger, A. 1979, Introduction to Solar Radio Astronomy and Radio Physics (Dordrecht: Reidel)
Kundu, M. R. 1965, Solar Radio Astronomy (New York: Wiley)
Kundu, M. R., & Vlahos, L. 1982, Space Sci. Rev., 32, 405
Kurths, J., & Schwarz, U. 1994, Space Sci. Rev., 68, 171
Makhmutov, V. S., Costa, J. E. R., Raulin, J.-P., Kaufmann, P., Lagrotta, P. R., Giménez de Castro, C. G., Magun, A., & Arzner, K. 1998, Sol. Phys., 178, 393
Makhmutov, V. S., Raulin, J.-P., Giménez de Castro, C. G., Kaufmann, P., & Correia, E. 2003, Sol. Phys., submitted
Mallat, S. G. 1989, IEEE Trans. PAMI, 11, 674
McClemments, K. C., & Brown, J. C. 1986, A&A, 165, 235
Melo, A. M., Giménez de Castro, C. G., Kaufmann, P., Levato, H., Marun, A., Pereyra, P., & Raulin, J.-P. 2002, in Proc. XXVIIth URSI General Assembly, Paper 2202
Melrose, D. B. 1994, ApJS, 90, 623
Ramaty, R. 1969, ApJ, 158, 753
Ramaty, R., Schwartz, R. A., Enome, S., & Nakajima, H. 1994, ApJ, 436, 941
Raulin, J.-P., Kaufmann, P., Olivieri, R., Correia, E., Makhmutov, V., & Magun, A. 1998, ApJ, 498, L173
Raulin, J.-P., Vilmer, N., Trottet, G., Nitta, N., Silva, A. V. R., Kaufmann, P., Correia, E., & Magun, A. 2000, A&A, 355, 355
Raulin, J.-P., Willson, R. F., Kerdraon, A., Klein, K.-L., Lang, K. R., & Trottet, G. 1991, A&A, 251, 298
Sturrock, P. A., Kaufmann, P., Moore, R. L., & Smith, D. F. 1984, Sol. Phys., 94, 341
Sturrock, P. A., & Uchida, Y. 1981, ApJ, 246, 331
Tajima, T., Brunel, F., & Sakai, J. 1982, ApJ, 258, L45
Tarbell, T. D., & Title, A. M. 1977, Sol. Phys., 52, 13
Trottet, G., Raulin, J.-P., Kaufmann, P., Siarkowski, M., Klein, K.-L., & Gary, D. E. 2002, A&A, 381, 694
Vilmer, N. 1987, Sol. Phys., 111, 207
Vlahos, L. 1995, in Coronal Magnetic Energy Releases, ed. A. O. Benz & A. Krüger (LNP 444; Heidelberg: Springer), 115
Yoshimori, M., et al. 1991, Sol. Phys., 136, 69
Zodi Vaz, A. M., Kaufmann, P., Correia, E., Costa., J. E. R., Cliver, E. W., Takakura, T., & Tapping, K. F. 1987, in SMM Topical Workshop on Rapid Fluctuations in Solar Flares, ed. B. R. Dennis, L. E. Orwig, & A. L. Kiplinger (NASA Conf. Proc. 2449; Washington, DC: NASA), 171